

Polarization properties of ion-excitation mechanisms in high-voltage gaps

E. Stambulchik and Y. Maron
Faculty of Physics, Weizmann Institute, 76 100 Rehovot, Israel

J. E. Bailey and M. E. Cuneo
Sandia National Laboratories, Albuquerque, New Mexico 87185
 (Received 17 October 2001; published 13 May 2002)

We investigate the excitation of atomic levels in a high-voltage discharge gap by studying the spectrum of the $2p$ - $3d$ transitions of Li I atoms flowing in the gap. The Stark splitting of this transition, due to the gap electric field, enables resolving the lines originating from different magnetic sublevels of the $3d$ level. We show that the atomic level populations are dominated by excitations due to ions accelerated in the gap. The directionality of the ion beam induces magnetic sublevel populations that are remarkably different from the statistical distribution, where the major role is played by the relatively low-energy ions accelerated near the ion-emitting surface. By accounting for the polarization properties of the beam-induced level excitations we were able to obtain good agreement with observed populations of atomic levels with different m_l values.

DOI: 10.1103/PhysRevA.65.052726

PACS number(s): 34.50.-s, 34.80.-i, 52.20.-j, 52.70.-m

I. INTRODUCTION

Experimental systems characterized by the acceleration of charged particles, such as ion accelerators and plasma diodes, are employed in various areas of research. In such devices, the energetic particles generally collide with other atomic species that are either present as an ambient gas or are externally injected. The collisions affect the atomic level populations of the excited atoms or ions, which then undergo the spontaneous emission that may serve for studying conditions in such devices. In the area of plasma physics, atomic emission spectroscopy in ion-accelerating gaps provides a tool for investigating various atomic-physics phenomena under high electric fields, such as the Stark effect [1–3], electric-field induced tunneling [4], and the reduction of transition probabilities [5,6]. Evidently, the spectra obtained in such experiments also provide diagnostics of the non-neutral plasma in the high-field acceleration gap.

The intensity of the spontaneous emission P between levels i and j is proportional to $n_i A_{ij}$, where n_i is the excited-state population density and A_{ij} is the Einstein coefficient. Therefore, accurate interpretations of line intensity measurements require knowledge of the population densities. Furthermore, the understanding of the level population mechanisms is a requirement for extracting information on transition probability “quenching” at higher fields [6].

Plasma polarization spectroscopy (PPS) [7] has recently become of an increasing interest. The idea behind PPS is that polarized light emitted by plasma may be used to infer the presence of an anisotropy in the electric or magnetic fields or in the particle velocity distributions. Provided that the underlying processes are sufficiently well understood, the light polarization can thus be used to infer the fields and/or the directionality of the particle trajectories in the plasma.

Spectral line emission originating from atoms or ions excited by particles whose velocity distribution is anisotropic is, in general, polarized, as has been known for almost a century [8]. The theory of such polarization phenomena was further developed and improved later on [9,10]. It has been

realized [11–16] that under conditions present in various plasma devices or environments, collision-induced level alignment by electron beams may be a source of observed polarization of the light emission. However, to the best of our knowledge, the role of ions in formation of orientation-dependent level populations in high-voltage gap devices has not yet been addressed.

In this paper, we describe an analysis that provides methods to interpret the polarized spectrum that was observed in one such experiment. A motivation for this work was the results of the high-electric-field measurements performed with the ion-beam diode SABRE [17], in experiments investigating the generation of lithium ion beams as a part of the ion-beam-fusion program. In these experiments, the charge exchange of Li II accelerated from the anode surface with neutral atoms in the immediate vicinity of the surface formed a stream of Li I moving from the anode toward the cathode of the accelerating gap [18]. Time- and space-resolved spectra from the Li I $2p$ - $3d$ transition from the gap were measured. Near the end of the pulse the average field in the gap is about 0.5 MV/cm, low enough to ensure negligible quenching for the radiative-decay rates of the Li I $2p$ - $3d$ transition and no field ionization of the $3d$ levels. However, such a field is still large enough for the blue-shifted and the red-shifted (those originating from the $3d$ $m_l=0,1$ and $m_l=2$ sublevels, respectively) Stark components of this transition to be resolved. The ratio of the intensities measured with the observation direction perpendicular to the electric field axis was $I_{0,1}/I_2=4.48\pm 0.22$, where $I_{0,1}$ and I_2 are, respectively, the intensities of the blue- and red-shifted components of the Li I $2p$ - $3d$ transition. This is a significant deviation from the theoretical value of $7/3$ calculated for conditions where the sublevels are statistically populated.

Here, we demonstrate that this observation can be explained by accounting for the polarization of the sublevel populations produced by the excitation conditions in the gap. An examination of plasma parameters in the diode showed that, for the specific conditions, the ion-beam collisional excitation is responsible for the formation of such polarization

properties. The dominant role of ions and, correspondingly, the negligible contribution of electrons in the level population formation, is due to the nature of high-power diodes. In these devices the typical electric fields are so strong that electrons are accelerated to energies very far in the cross-section asymptotic region corresponding to extremely low excitation rates, while the ions move with relatively low velocities, that lead to correspondingly high excitation rates. Differences between the ion-excitation rates for different sublevels produce sublevel populations that are consistent with the measured intensity ratio.

The experimental setup is described in Sec. II, a detailed description of the model is given in Sec. III, and the numerical calculations and results are presented in Sec. IV. The results are then discussed in Sec. V, including considerations of other effects that could cause the anomalous sublevel populations.

II. EXPERIMENT

The experiments were performed with an applied magnetic-field extraction-geometry ion diode powered by the SABRE accelerator [17]. The cylindrically symmetric diode configuration is shown in Fig. 1. In the extraction geometry, ions born at the annular ring anode are accelerated along the direction of the cylindrical axis by an applied voltage pulse. The SABRE diode in these experiments used an 11.3-mm anode-cathode (AK) gap and inner and outer anode radii of 44 mm and 64 mm, respectively. The voltage pulse duration is typically 40 nsec and it peaks at ≈ 4 MV. A 2 T magnetic field in the radial direction (roughly parallel to the anode) prevents electrons born at the physical cathode from crossing directly to the anode. The electrons $\mathbf{E} \times \mathbf{B}$ drift in the annular direction, forming a cloud that fills the cathode side of the diode. This electron cloud is known as a virtual cathode. Ions are accelerated between the anode and the virtual cathode, passing through the virtual cathode as they exit the diode.

The results reported here were obtained during studies of laser-initiated lithium ion sources [19]. A 10-nsec full-width at half-maximum, $1.06 \mu\text{m}$ wavelength Nd:YAG (yttrium aluminum garnet) laser pulse was injected along the cylinder axis and directed onto the anode using a conical mirror. The laser illuminates the anode with an $\approx 10^7$ – 10^8 W/cm² irradiance, forming a plasma that can supply ions to the acceleration gap. The anode surface is a LiAg alloy, specially formulated to promote the ability to control the adsorption of contaminants.

The focus of the present paper is on the atomic physics information obtained during the ion diode experiments. The behavior of the diode with this ion source is complex and the measurements of the diode performance will be reported elsewhere. However, a qualitative description of the physics governing the diode operation is needed in order to exploit the unique atomic physics opportunities that are present. A schematic diagram of the important physical processes is shown in the Fig. 1 inset.

Optimum diode performance is believed to require a laser fluence adequate to fully ionize the anode plasma. Otherwise, as ions are accelerated through the remaining neutrals,

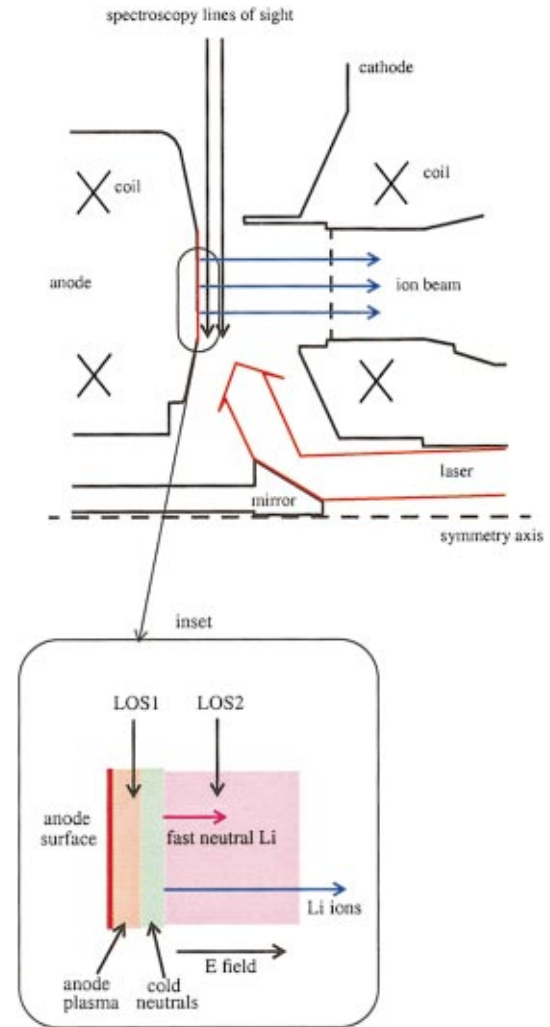


FIG. 1. (Color) Schematic diagram of the cylindrically symmetric SABRE ion diode. The inset illustrates the physical processes near the anode that launch lithium atoms into the acceleration gap. LOS1 and LOS2 are spectroscopy lines of sight at 0.5 and 3.0 mm from the anode surface, respectively.

they undergo charge exchange [20]. The charge-exchange neutral atoms retain the energy of the ions at the instant of the charge exchange, typically 10–50 keV [18], which is sufficient for the charge-exchange neutral atoms to fill the diode gap on the time scale of the diode pulse. Subsequent ionization of the charge-exchange neutrals atoms can divert the diode current away from the desired ion beam or it can even lead to an AK gap breakdown, if the charge-exchange neutral atom density is large enough.

The neutral Li I atoms injected into the gap begin with a population distribution that depends on the details of the charge-exchange process that creates them. They then encounter both the relativistic electrons and the beam ions flowing in the gap. The collisions cause excitations and de-excitations of the Li I levels. Another mechanism contributing to the level population dynamics is radiative decay. The emitted light is collected by the optical system.

Spectra were acquired using two separate time-resolved optical spectrographs [21,22]. A lens-coupled fiber-optic ar-

ray collected light from an array of 1-mm-diameter spots, with the optical line-of-sight axis oriented parallel to the anode surface along a chord positioned at a 54 mm radius. The fiber diameter was 100 μm and the 50-mm-focal-length lens provided a magnification of 0.1. The collection numerical aperture was 0.011. One spectrograph system collected light from a spot centered at 0.5 mm from the anode surface and the other collected light from a spot centered at 3.0 mm (see Fig. 1). The light was transported from the diode region to a remote screen room using a 39.6-m-long fiber-optic link. The spectra are insensitive to the polarization of the light generated in the diode due to mixing of the polarizations as the light propagates through the fiber. The end of each fiber is coupled to a 1-m-focal-length Czerny-Turner spectrograph equipped with a 300 l/mm grating that provided a reciprocal dispersion of 33 $\text{\AA}/\text{mm}$. A streak camera with a 40-mm-long photocathode spanning a 1300 \AA range recorded the spectrum with a 1-nsec time resolution and 5.5 \AA spectral resolution. As in previous measurements [2], the precision of wavelength shift measurements was about ten times better than the spectral resolution.

The spectroscopic data reported here were obtained in an experiment that used a relatively low laser power, such that the Li I density in the gap due to charge exchange was larger than desired for optimum diode performance. However, this enabled measurements of the Li I $2p\text{-}3d$ transition with excellent signal-to-noise ratio. Thus, data suitable for expanding knowledge of atomic physics can be extracted even from experiments with below-optimum ion-beam production. In this experiment, measurements of the Li velocities were not performed. The detailed study [18] of the lithium atom velocities in the anode-cathode gap, performed on a different diode with a LiF anode for which no laser was used to produce the anode plasma, showed that the Li atoms are essentially monoenergetic, moving with $\approx 50\text{--}70$ $\text{cm}/\mu\text{s}$ velocities, corresponding to ≈ 10 keV. For our case, the numbers may need to be scaled down according to the lower fields we deal with here, resulting in neutral Li I energies of the order of a few keV. A lower bound for the atomic Li velocity can be derived based on the fact that it should be high enough to cross the gap (at least, to the second line of sight) during the pulse duration, giving ≈ 10 $\text{cm}/\mu\text{s}$. For these calculations we, therefore, use velocities of 20 $\text{cm}/\mu\text{s}$, and then examine the sensitivity of our solutions to a twofold variation in this parameter.

A qualitative description of the Li I $2p\text{-}3d$ spectra obtained in high-power diode experiments has been previously reported [5,6]. In the present experiment the spectra from the fiber positioned nearest the anode exhibited continuum and unshifted spectral lines that indicate the formation of anode plasma. While interesting for diode physics, this information is not used for the atomic physics studies reported here. A portion of the time-resolved spectrum obtained from the fiber positioned at 3.0 mm from the anode in the present experiment is shown in Fig. 2. Early in the diode pulse the electric field is 5–10 MV/cm, the $3d$ level is field ionized, and $2p\text{-}3d$ emission is not observed. This initial phase, designated δt_1 in Fig. 2, is the period when an intense ion beam is generated. In the middle of the diode pulse the electric field

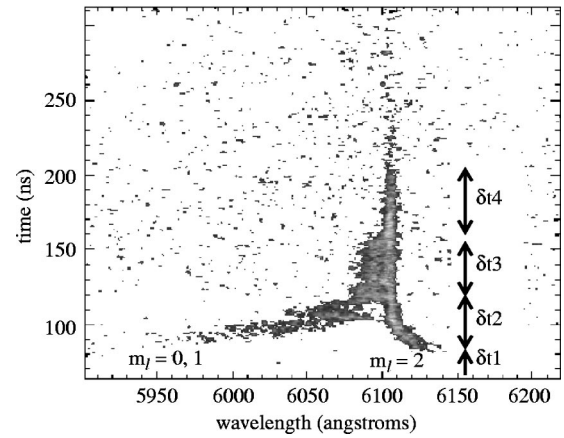


FIG. 2. A portion of the time-resolved spectrum measured at 3.0 mm from the anode in SABRE experiment no. 1892. The initial high-field diode phase, when the Li $3d$ is field ionized, is denoted by δt_1 . The phase of 1–4 MV/cm field is denoted by δt_2 . The 0.2–1.0 MV/cm phase, addressed in this paper, is denoted by δt_3 . As the diode electric field vanishes (δt_4), the Li I $2p\text{-}3d$ components merge into one unshifted line. The times given are with respect to an arbitrary reference.

is 1–4 MV/cm and the $2p\text{-}3d$ is observed with a Stark-split pattern spanning up to 100 \AA (δt_2 in Fig. 2). During this phase, the details of the observed pattern may provide information regarding both field-ionization rates and transition probability quenching [4–6]. These data will be published elsewhere. The focus of the present paper is the third phase of the diode pulse when the electric field is below 1 MV/cm (δt_3 in Fig. 2). During the third phase the $2p\text{-}3d$ line is still split into two resolvable components corresponding to the $m_l=0,1$ and $m_l=2$ upper levels. A lineout averaging over a 4-nsec interval during the third phase is shown in Fig. 3. A fit obtained with the ROBFIT [23] line fitting code is superimposed on the data. The relative intensity of the two components was measured to be 4.48 ± 0.22 by computing a weighted mean of the ROBFIT results from a sequence of lineouts taken over the 28 nsec duration of phase three.

III. THEORETICAL MODEL

We first consider the relative importance of electrons and ions in populating the sub-levels of the Li I $3d$ level. Based on the dominance of the ion excitations shown, the rate equations for processes populating the various sublevels by the ion beam are constructed, the solution of which gives the population densities as a function of the time and space in the gap. The rate equations are initially formulated assuming monoenergetic lithium atoms flowing in the gap, excited by a singly ionized lithium beam accelerated in the diode gap. Further, considerations will be presented discussing a generalization of this scheme.

A. Relative importance of electrons and ions

We first demonstrate the negligible role of $e\text{-Li}$ collisions in the lithium atom excitations. Since collision losses in the

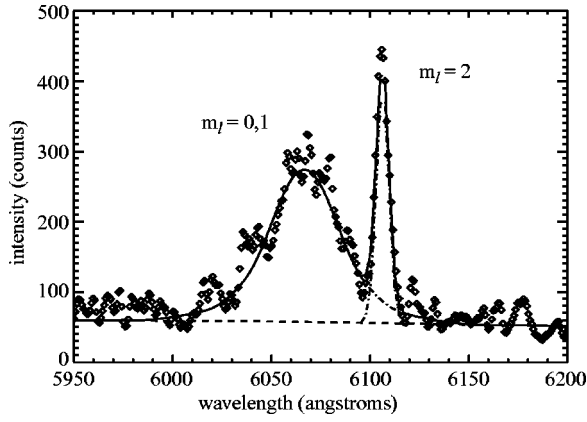


FIG. 3. Lineout averaging over a 4-nsec interval during the δt_3 phase shown in Fig. 2. The experimental data are shown as diamonds, the fits to the individual line components are dot-dash lines, the background is a dashed line, and the composite fit is shown as a solid line.

diode gap are negligible, the energies of the ions and electrons at a distance x from the anode are

$$E_I = U(x) \quad (1)$$

and

$$E_e = U_o - U(x), \quad (2)$$

respectively, where $U(x)$ is the self-consistent potential in the diode gap, assuming zero potential at the anode. Since the energy of the electrons sufficiently far from the cathode is very high, the e -Li I cross section for a given transition is very small, approximated by the well-known $\sim \ln(E)/E$ or $\sim 1/E$ asymptotes for dipole-allowed or dipole-forbidden transitions, respectively. The Li^+ -Li cross-section behavior, since the ion energy is much closer to the threshold for excitation, can be estimated by scaling the e -Li cross-section:

$$\sigma_{\text{Li}^+-\text{Li}}(E) \approx \sigma_{e-\text{Li}}\left(\frac{m}{M}E\right), \quad (3)$$

where m and M are the electron and the ion mass, respectively. The equivalent (scaled) energy of the Li ions is thus ≈ 100 eV, even when the ions reach the cathode.

Comparing the collision rate ν , given by $n\sigma v$ for ions and electrons, and neglecting the unimportant $\ln(E)$ factor, one finds that

$$\frac{\nu_i}{\nu_e} \approx \sqrt{\frac{E_e}{E_I}} \sqrt{\frac{M}{m}}. \quad (4)$$

In the middle of the gap, where energies of the ions and electrons are comparable, the ionic contribution is thus about 100 times larger than the electronic one. Closer to the cathode, the ratio decreases, but only very close to the cathode does the electron collision rate become comparable to the ion collision rate. This cathode region has not been studied in the experiments addressed here.

Formula (4) assumes the cross sections are far beyond the threshold. However, since the ion and neutral beams originate at the anode surface and propagate in the same direction, a noticeable part of the drift path of the neutral lithium (near the anode) corresponds to collisions with relatively slow ions. Further, we will show that the populations of the Li I $3d$ sublevels are mainly established during this phase, while during the rest of the Li I flight (as the colliding ions become more energetic and, therefore, the collisional cross sections drop sharply) the level populations become dominated by the $3d-2p$ radiative decay process. Narrowing down our attention to the near-anode region, where the equivalent scaled ion beam energy is of the order of the transition threshold E_o , we can assume an approximately constant cross section σ_o for the Li^+ -Li collisions. The electrons in the same region reach almost the entire eU_o energy, therefore, the ion to electron collisional excitation rate ratio near the anode surface is

$$\frac{\nu_i}{\nu_e} \approx \sqrt{\frac{eU_o}{E_o}} \sqrt{\frac{m}{M}}, \quad (5)$$

giving $\approx 10^3$.¹ Thus, we here only consider the Li^+ -Li collisions for calculations of the Li I excited-level populations.

B. Rate equations

To calculate the Li I level populations we account for collisional excitations, collisional deexcitations, and radiative decays. The population N_i of the Li I i th state is given by

$$\frac{dN_i}{dt} = \sum_{j \neq i} (-N_i \nu_{ij} + N_j \nu_{ji} - N_i A_{ij} + N_j A_{ji}), \quad (6)$$

where ν_{ij} stands for a collisional transition rate from the state i to the state j ($i < j$ and $i > j$ correspond to excitation and deexcitation processes, respectively). To account for polarization effects, one has to distinguish between the magnetic sublevels, therefore, i is characterized by the $|nlm_i\rangle$ set of quantum numbers (we neglect the fine structure, since the Stark splitting of the Li I $3d$ level caused by an electric field as low as 100 kV/cm considerably exceeds the spin-orbit interaction effects — see, e.g., [3]).

The ν_{ij} rates are functions of time, since the ion-beam energy varies along the ion-beam path. Using the neutral beam of a velocity v_o as the reference frame, one obtains

$$\nu_{ij} = n_I \sigma_{ij}(E'_I) v'_I, \quad (7)$$

where n_I is the ion-beam density, and v'_I and E'_I stand for the ion velocity and energy in this reference frame, i.e., $v'_I = v_I - v_o$, and $E'_I = M v_I'^2/2$. The accelerated ions in the beam are much faster than the Li I atoms, therefore, $v'_I \approx v_I$ and

¹Strictly speaking, the electrons near the anode are already relativistic, and the cross sections deviate from the Born asymptotes by some numeric factor. Therefore, the above ratio is probably a few times smaller.

$E'_i \approx E_i \equiv U(v_o t)$. In addition, the $n_I v_I$ product is J_D/e , where J_D is the diode current, carried by the (singly charged) Li^+ ions. Using Eq. (6), we thus obtain

$$\frac{dN_i}{dt} = \sum_{j \neq i} \left(\frac{J_D}{e} [-N_i \sigma_{ij}(U(v_o t)) + N_j \sigma_{ji}(U(v_o t))] - N_i A_{ij} + N_j A_{ji} \right). \quad (8)$$

In the present system, the atoms (the level populations of which are described by the rate equations) move with the velocity v_o from the anode to the cathode. The population densities $N_i(t)$ determine the emission spectra of the lithium atoms as a function of the distance from the anode surface as these atoms move from the anode to the cathode. In order to track the populations as the atoms travel across the gap, the differential equations should be re-written to describe N_i as functions of the space coordinate $x = v_o t$ rather than of time. For the case of monoenergetic atoms (moving with a velocity v_o) this transformation is made by substituting x for $v_o t$, i.e.,

$$\frac{dN_i}{dx} = \frac{1}{v_o} \sum_{j \neq i} \left(\frac{J_D}{e} [-N_i \sigma_{ij}(U(x)) + N_j \sigma_{ji}(U(x))] - N_i A_{ij} + N_j A_{ji} \right). \quad (9)$$

C. Possible extensions

Let us consider some generalizations of the solution presented in the preceding section. First, the neutral Li I beam is not necessarily monoenergetic. Instead, one can assume that the velocity distribution in the beam is governed by a probability distribution function $P(v)$, such that $\int dv P(v) = 1$. Then, the correct level populations can be expressed as

$$N_i(x) = \int dv P(v) N_i(v, x), \quad (10)$$

where $N_i(v, x)$ denotes the i th solution (i.e., the population of the i th level as a function of the distance from the anode) of the set of equations (9) solved for $v_o = v$.

Similarly, the ion beam may consist of several species that differ by charge states and masses. The set of equations (9), generalized for this case, is given below:

$$\frac{dN_i}{dx} = \frac{1}{v_o} \sum_{j \neq i} \left(\sum_s \frac{J_s}{Z_s e} [-N_i \sigma_{ij}^s(U(x)) + N_j \sigma_{ji}^s(U(x))] - N_i A_{ij} + N_j A_{ji} \right). \quad (11)$$

Here, s stands for a component of the ion beam produced by a species with a charge Z_s , yielding the full diode current $J_D = \sum_s J_s$, and σ_{ij}^s denotes the cross section relevant for collisions with this species.

A more interesting class of phenomena relates to the ‘‘A-quenching’’ effects. It is known (e.g., [24]), and has been

observed [5,6], that the matrix elements, and hence, the oscillator strengths, change when a sufficiently strong electric field is applied. Consequently, the values of the Einstein coefficients A_{ji} are altered by the applied electric field. An equally important effect that also stems from the changes in the matrix elements under the electric field is that, since the cross sections directly depend on the matrix elements, they should experience a similar ‘‘quenching.’’ Thus, both the Einstein coefficients and the cross sections should be modeled as dependent on the electric field $F(x)$ at any given point x :

$$\frac{dN_i}{dx} = \frac{1}{v_o} \sum_{j \neq i} \left(\frac{J_D}{e} [-N_i \sigma_{ij}(F(x), U(x)) + N_j \sigma_{ji}(F(x), U(x))] - N_i A_{ij}(F(x)) + N_j A_{ji}(F(x)) \right), \quad (12)$$

where $F(x) = -dU/dx$. For yet higher electric fields, when tunneling to continuum states start to play an important role [25], one has to take into account the field ionization too.

IV. RESULTS

The set of the differential equations (8) was solved numerically. In the numerical calculations, we used the following set of Li I states: $2s$, $2p$, $3s$, $3p$, $3d$, and $4f$, all including their magnetic sublevels. The $4f$ level (the only level beyond the $n=2$ and $n=3$ levels) was also included because of its strong collisional (de)excitation rates with $3d$. The Einstein coefficients A_{ij} were taken from [26]. To the best of our knowledge, there are no data, either theoretical or experimental, available for the collisional $\text{Li}^+ - \text{Li } m_l$ -resolved cross sections. We thus used the respective electron-Li cross sections, scaled according to Eq. (3), and for energies below the respective (scaled) e -Li threshold we used a simple, $\propto E$ extrapolation (the validity of such a substitution will be discussed in the following section). The e -Li cross sections in the $|nlm_l\rangle$ basis were calculated with a computer code [27] that utilizes the convergent close-coupling (CCC) method.

For brevity, we here present only a few of the calculated cross sections. The most important mechanisms populating the $3d$ level are the direct excitation from the ground state and the $2p$ - $3d$ excitation. In the latter case, the polarization of the $3d$ level also depends on the polarization of the $2p$ level, and, therefore, on the polarization properties of the $2s$ - $2p$ excitation process. The $2s$ - $2p$ cross sections as a function of energy are given in Fig. 4. The total cross section is given in Fig. 4(a), and the relative weights of the collisions between specific m_l are plotted in Fig. 4(b). In the latter, the dashed line corresponds to the absence of a polarization, i.e., when all three possible collisional transitions ($2s_0$ - $2p_0$, $2s_0$ - $2p_{+1}$, and $2s_0$ - $2p_{-1}$) are equally possible. The cross-section data obtained for the $2s$ - $3d$ and $2p$ - $3d$ transitions are presented in a similar manner in Figs. 5 and 6, respectively, (in the case of the $2p$ - $3d$ transitions we summed over

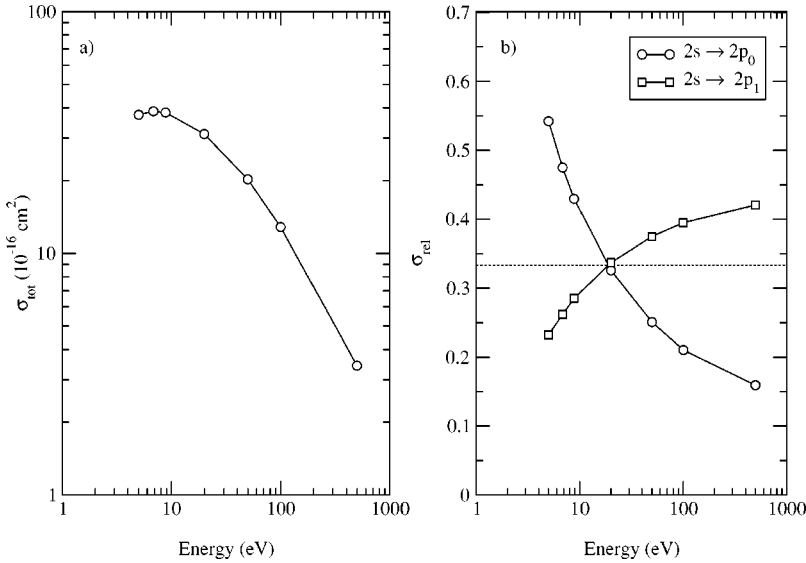


FIG. 4. Li I $2s$ - $2p$ electron excitation cross sections: (a) total cross section; (b) relative cross sections between sublevels.

the different m_l of the initial states, for the clarity of the graph). All the cross sections exhibit pronounced polarization features. It is seen that in the region of the lower energies, the preferred channels of excitations are those with $\Delta m_l = 0$, while cross sections at the higher energies tend to favor transitions with the highest Δm_l possible.

We use the space-charge-limited potential $U(x) = U_o(x/d)^{3/2}$ (where d is the diode gap width and U_o is the diode voltage) since this is a satisfactory approximation for the diode region near the anode. The values of d and U_o have no importance as long as their combination provides an electric field strength, given by $F(x) = \frac{3}{2} U_o/d(x/d)^{1/2}$, in agreement with the measured value (of ≈ 1 MV/cm). We use the neutral Li velocity $v_o = 2 \times 10^7$ cm/sec (value that was discussed in Sec. II) and the ion-beam flux $J_D = 1.3 \times 10^{21}$ cm $^{-2}$ sec $^{-1}$.

The results of the calculations depend on the initial populations of the Li I atoms produced by the charge-exchange processes. These initial populations are not known experimentally. Since the energy of the neutral Li atoms is believed

to be low, it is quite possible that the mechanism responsible for the neutral beam production is a resonant charge-exchange process. Although the resonant charge-exchange cross section peaks at as low energy as ≈ 100 eV, it could produce enough ≈ 1 keV Li I, provided that the neutral atom layer in which the charge exchange occurs is sufficiently wide. Alternatively, the dominant mechanism for the Li I production might be the nonresonant charge exchange. It appears that resonant and nonresonant processes may both contribute to the initial Li I population.

If the resonant charge-exchange process plays a major role in the Li I formation, one should expect the initial $2s:2p:3d$ level population ratio to be 1:0.06:0.004 [28] (as mentioned above, the major mechanisms of the $3d$ sublevel population dynamics are the $2s$ - $3d$ and $2p$ - $3d$ collisional excitations, therefore, the initial populations of other levels play a negligible role). The energies of interest here are at or slightly below the lower bound of the energy region used in the Ref. [28], therefore, we used a simple extrapolation (justified by the smooth energy dependence in this region). On

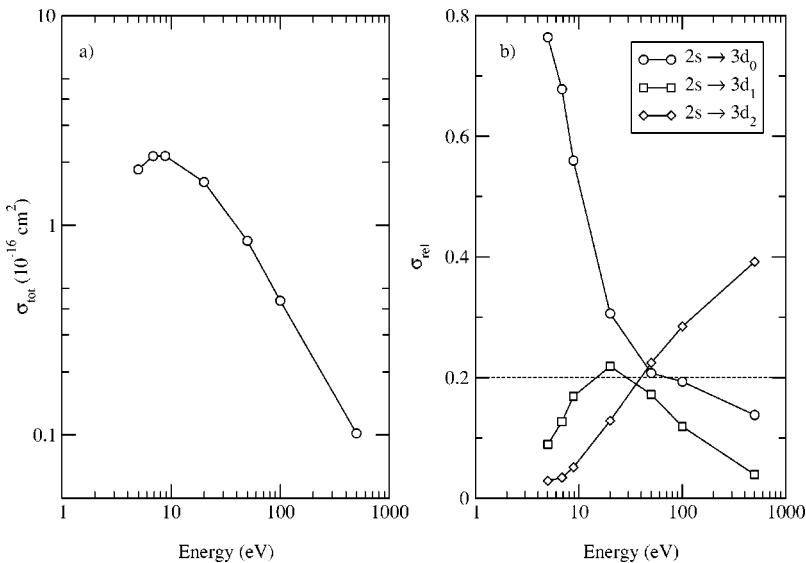


FIG. 5. Li I $2s$ - $3d$ electron excitation cross sections: (a) total cross section; (b) relative cross sections between sublevels.

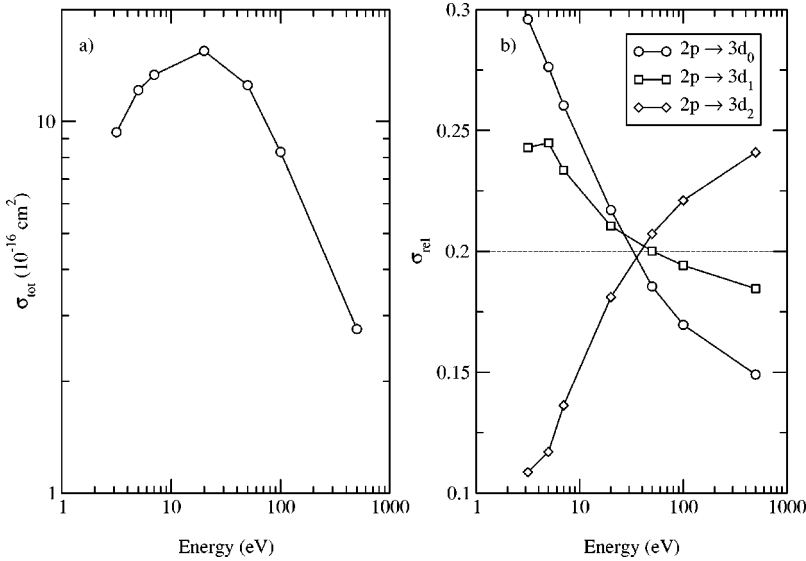


FIG. 6. Li I $2p$ - $3d$ electron excitation cross sections: (a) total cross section; (b) relative cross sections between sublevels.

the other hand, if the neutral atoms are produced largely by the nonresonant charge exchange, the initial $2s:2p:3d$ level population ratio is expected to be $\approx 1:0.3:0.03$ [29,30].

With these uncertainties in the initial level densities of the Li I streaming in the gap, we examine our solution under several assumptions on the initial level populations. Below, we give a few examples that cover a range of initial population values.

In Figs. 7–9 the populations of the Li I $3d$ sublevels are presented as functions of the distance from the anode. For these runs, we assumed that the $2s:2p:3d$ initial level populations are in the $1:0.06:0.004$, $1:0.3:0.03$, and $1:0.1:0.01$ ratios, respectively. The initial populations in Figs. 7 and 8 correspond to the resonant and nonresonant charge-exchange processes, respectively, in keeping with the estimates mentioned above, and Fig. 9 corresponds to an intermediate case. From the figures, one can see a remarkable polarization of the $3d$ level over almost the entire diode gap. The polarization dynamics of the Li I $3d$ level can be roughly split into three phases. The first, near the anode (up to ~ 1 mm), is characterized by very low energies of the ions with the corresponding excitation and deexcitation cross sections being almost zero, therefore, the dominant mechanism of the sublevel populations is the radiative decay. Over the following several millimeters, ions gain enough energy for the collisional (de)excitation rates to become comparable to or exceed the radiative decay rates. Since, as we showed earlier (Figs. 4–6), the cross sections for this energy region exhibit a strong preference for the transitions with $\Delta m = 0$, the populations of the $3d_0$ and $3d_1$ sublevels start to dominate the $3d_2$ population, mainly due to the $2s$ - $3d_0$, $2p_0$ - $3d_0$, and $2p_1$ - $3d_1$ excitation channels. It is the second phase (at the distance ≥ 1 mm from the anode), in which the polarization of the $3d$ level reaches its maximum. In the third phase, further towards the cathode, the ions are fast enough to cause the cross sections to drop, making the role of collisions (compared to the radiative decay) less important. In fact, at these ion energies also the preference becomes for excitation transitions with $\Delta m \neq 0$, altogether causing the polarization of the $3d$ level to disappear in the third phase.

In the present experiment, the value measured is the intensity ratio of the blue-shifted to the red-shifted Li I $2p$ - $3d$ components, i.e., $I_{0,1}/I_2$, observed in the direction perpendicular to the quantization axis. This value is readily expressed via the sublevel populations and 3 - j kinematic factors,

$$\frac{I_{0,1}}{I_2} \equiv \frac{I_{2p-3d_{0,\pm 1}}}{I_{2p-3d_{\pm 2}}} = \frac{\frac{1}{4}N_{3d_0} + \frac{9}{20}N_{3d_1}}{\frac{3}{10}N_{3d_2}}. \quad (13)$$

The blue to red intensity ratio, calculated for the three different sets of initial conditions, is presented in Fig. 10. On the same graph, the dashed line denotes the case of the absence of polarization, i.e., $7/3$, according to Eq. (13). The weighted average of the experimental data (measured at 3

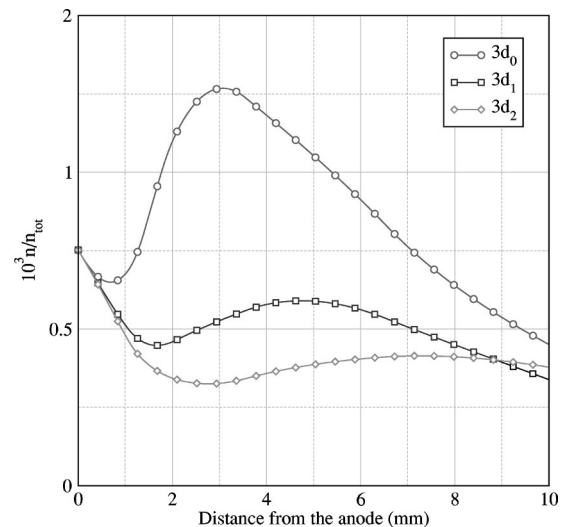


FIG. 7. The populations (relative to 1) of the Li I $3d$ sublevels assuming the initial $2s:2p:3d$ level population ratio is $1:0.06:0.004$, corresponding to the resonant charge-exchange mechanism.

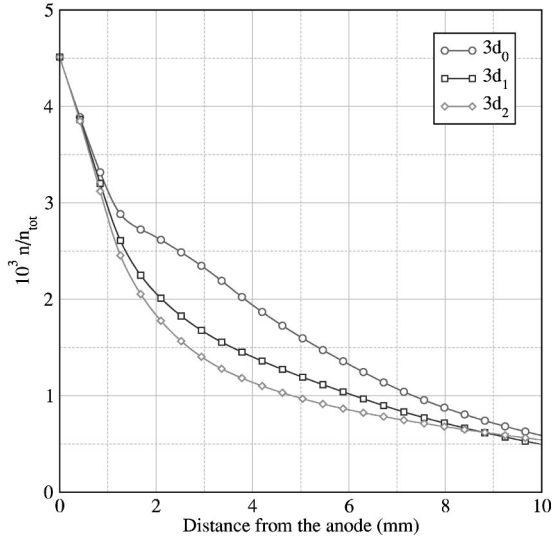


FIG. 8. The populations (relative to 1) of the Li $3d$ sublevels assuming the initial $2s:2p:3d$ level population ratio is 1:0.3:0.03, corresponding to the nonresonant charge-exchange mechanism.

mm from the anode) with its error bars is also given. Based on these results, we believe that the initial Li $3d$ level population ratio is close to 1:0.1:0.01.

V. DISCUSSION

A. Insensitivity of the qualitative picture to the parameters used

It should be emphasized that the qualitative picture of the results here presented is insensitive to the parameters used within a reasonable range of values. To illustrate this, we present several examples showing the dependence of the sublevel populations on the various parameters.

As shown above, the parameter values that appear to be the most probable are as follows: the space-charge-limited potential law with 1 MV/cm at 3 mm from the anode, the

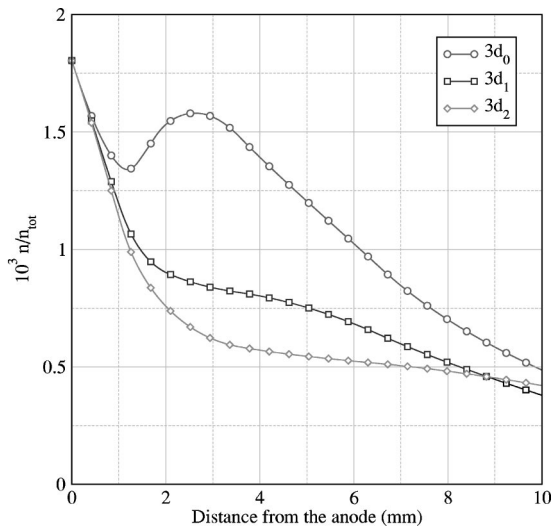


FIG. 9. The populations (relative to 1) of the Li $3d$ sublevels assuming the initial $2s:2p:3d$ level population ratio is 1:0.1:0.01.

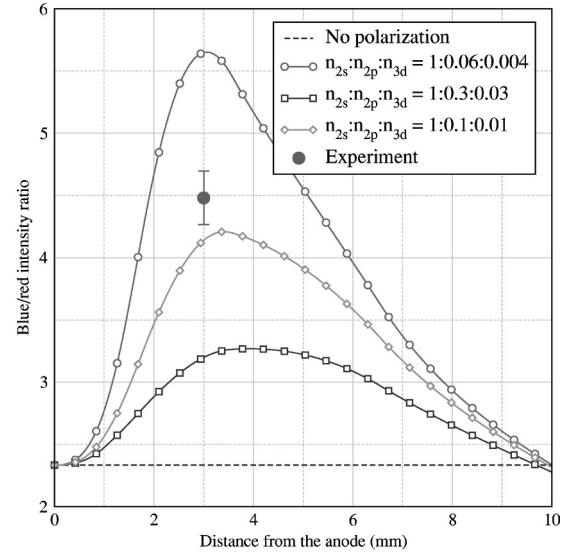


FIG. 10. The blue to red intensity ratio, calculated for the three different sets of initial conditions. The dashed line denotes the case of the absence of polarization. The experimental data are indicated.

neutral Li velocity $v_o = 2 \times 10^7$ cm/sec, the ion-beam flux $J_D = 1.3 \times 10^{21}$ cm $^{-2}$ sec $^{-1}$, and the 1:0.1:0.01 $2s:2p:3d$ initial population ratio. These are the parameters used to produce Fig. 9 and the third curve in Fig. 10.

Calculations corresponding to twofold variations in the following parameters were performed: the electric field strength (0.5 MV/cm and 2 MV/cm), the neutral beam velocity v_o (1×10^7 cm/sec and 4×10^7 cm/sec), and the ion-beam flux J_D (6.5×10^{20} cm $^{-2}$ sec $^{-1}$ and 2.6×10^{21} cm $^{-2}$ sec $^{-1}$). Finally, since the potential dependence on the distance from the anode surface is not well known, we performed calculations assuming a linear dependence, $U_o x/d$ [rather than the $U_o(x/d)^{3/2}$ dependence]. The blue to red ratio curves corresponding to these calculations are presented in Fig. 11.

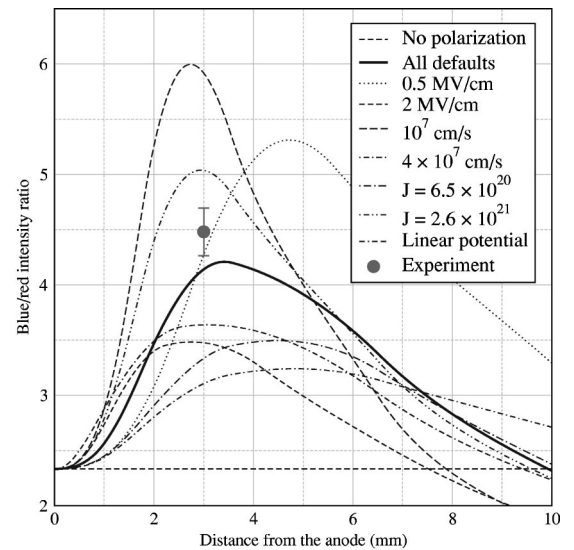


FIG. 11. The blue to red intensity ratio, calculated for a twofold variation of several parameters of the model.

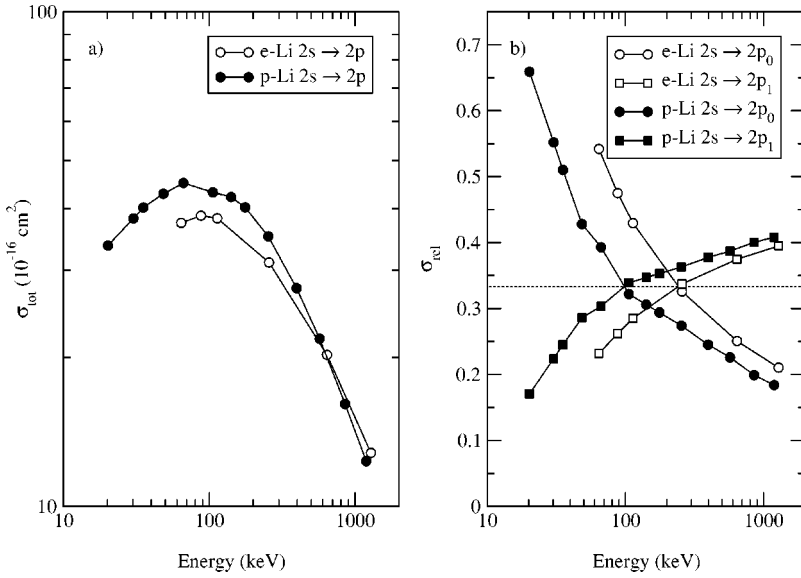


FIG. 12. Comparison of the $e\text{-Li}$ and $p\text{-Li}$ $2s-2p$ excitation cross sections, scaled to correspond to the Li^+ velocity.

From these examples, one can conclude that the qualitative predictions of the model presented here are insensitive to the various parameters of the experiment that are either not fully known or vary in time and/or are spatially inhomogeneous. Although the absolute values of the sublevel populations, and hence, the intensity of the emitted light, depend on the diode voltage and the neutral beam velocity, the polarization effects remain prominent.

B. Accuracy of the results

As it was mentioned in Sec. IV, the main source of uncertainties in the calculations is the use of the scaled $e\text{-Li}$ cross sections for the $\text{Li}^+\text{-Li}$ cross sections. Such scaled cross sections are obviously valid in the region where the Born approximation is justified, i.e., in the region of high (well above the peak cross section) energies. Moreover, the region around the peak cross section could generally be used with a fair confidence [31]. However, the region of low energies

near the threshold [of the effective scaled energy as defined in Eq. (3)] should be examined critically. For the $2s-3d$ and $2s-2p$ transitions, it was possible for us to compare the $e\text{-Li}$ cross sections with the $p\text{-Li}$ cross sections, calculated [32] using an atomic orbital CCC-based code. While the true $\text{Li}^+\text{-Li}$ cross sections may still, at low energies, deviate from the appropriately scaled $p\text{-Li}$ cross sections due to the internal structure of the Li^+ projectile [31,32], the comparison is nonetheless valuable. In Figs. 12 and 13, the $e\text{-Li}$ and $p\text{-Li}$ excitation cross sections of the $2s-2p$ and $2s-3d$ transitions are compared, respectively. As is expected, both the total and the relative cross sections coincide in the limit of high energies, while in the low-energy region the behavior is quite different in details. However, the tendency that the excitation probability is significantly larger for magnetic sub-levels with $m_l=0$ is the same for both the $e\text{-Li}$ and $p\text{-Li}$ excitation processes. This raises our confidence in using the scaled $e\text{-Li}$ (instead of the unavailable $\text{Li}^+\text{-Li}$) cross sections in the data analysis given above.

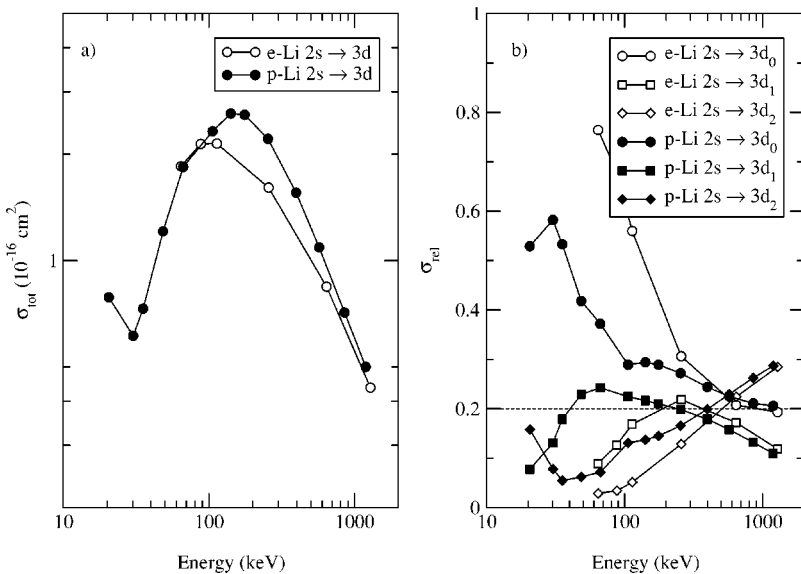


FIG. 13. Comparison of the $e\text{-Li}$ and $p\text{-Li}$ $2s-3d$ excitation cross sections, scaled to correspond to the Li^+ velocity.

C. Exclusions of other explanations

We have attempted to exclude other effects that could possibly affect the analysis presented above. First, the polarization properties of the optical detection system could not affect the data since the light collected from the plasma loses any polarization in its propagation through the long optical fiber.

As was mentioned above, the reduction of the oscillator strengths under the electric fields could be concurrent to the described process. However, the role of such a reduction in this data analysis is negligible due to the relatively weak electric field. It can be argued, though, that the reduction in the oscillator strengths and the field ionization may influence the level populations at earlier times (close to the beginning of the pulse), affecting the blue to red ratio at later times. However, since the $m_l=0$ sublevel is ionized at a lower field than the $m_l=1$ and $m_l=2$ sublevels, as was shown both experimentally [5,6] and theoretically [4], field ionization, if any, would tend to lead to even lower blue to red ratios in the experiment.

We note that, in principle, it is possible that the charge-exchange process producing the fast Li atoms propagating in the diode gap may result in the polarization of the $3d$ level at the immediate vicinity of the anode surface. However, the lack of data available for m_l -resolved $\text{Li}^+\text{-Li}$ (or $\text{Li}^+\text{-H}$) charge-exchange rates does not allow an analysis of this possibility to be made.

VI. SUMMARY

We have shown the importance of ion-atom collisions in the dynamics of the level populations of atomic species present in high-voltage accelerating gaps. The directionality of the ion beam in such devices induces a remarkable polarization of the atomic level population densities.

By analyzing such polarizing ion-atom excitations in a high-voltage ion diode, we were able to explain the observed strong polarization properties of the plasmas produced in the diode. Numerous calculations performed show that the qualitative picture of the polarization effect remains largely insensitive to such parameters as the diode voltage and the velocity of the neutral beam in the diode.

Due to the absence of the m -resolved $\text{Li}^+\text{-Li}$ cross sections, we used the scaled electron-Li I cross sections. While such a substitution is justified to give the correct qualitative tendency, it may cause uncertainties in the quantitative results. Therefore, it is highly desirable to use measured or calculated $\text{Li}^+\text{-Li}$ cross sections when these become available.

ACKNOWLEDGMENTS

We want to thank Professor I. Bray for providing us with his CCC code, Dr. J. Schweinzer for sharing with us unpublished results of his p -Li cross-section calculations, Professor H. Griem for fruitful discussions and critical comments on the manuscript, Professor R. K. Janev for valuable comments, and Dr. Yu.V. Ralchenko for his help in running the CCC code. This work was supported in part by the Minerva Foundation, Munich, Germany and the US-Israeli Binational Science Foundation, Jerusalem. The measurements described here were the result of a dedicated effort by the SABRE accelerator team. We especially acknowledge laser operation by R. G. Adams and B. F. Clark and spectroscopy instrumentation operation by A. L. Carlson and P. W. Lake. The authors thank J. P. Quintenz, M. K. Matzen, R. J. Leeper, and T. A. Mehlhorn for continuous support and encouragement. Sandia is a multiprogram laboratory operated by Sandia Corporation, a Lockheed Martin Company, for the U.S. Department of Energy under Contract No. DE-AC04-94AL84000.

-
- [1] Y. Maron, M.D. Coleman, D.A. Hammer, and H.S. Peng, *Phys. Rev. A* **36**, 2818 (1987).
 - [2] J.E. Bailey, A.B. Filuk, A.L. Carlson, D.J. Johnson, P. Lake, E.J. McGuire, T.A. Mehlhorn, T.D. Pointon, T.J. Renk, W.A. Stygar, and Y. Maron, *Phys. Rev. Lett.* **74**, 1771 (1995).
 - [3] E. Stambulchik and Y. Maron, *Phys. Rev. A* **56**, 2713 (1997).
 - [4] D. Fisher, Y. Maron, and L.P. Pitaevskii, *Phys. Rev. A* **58**, 2214 (1998).
 - [5] J.E. Bailey, A.B. Filuk, A.L. Carlson, D.J. Johnson, P. Lake, E.J. McGuire, T.A. Mehlhorn, T.D. Pointon, T.J. Renk, W.A. Stygar, Y. Maron, and E. Stambulchik, in *Atomic Processes in Plasmas*, edited by A.L. Osterheld and W.H. Goldstein, AIP Conf. Proc. No. 381 (AIP, Woodbury, NY, 1996), p. 245.
 - [6] J.E. Bailey, A.B. Filuk, A.L. Carlson, D.J. Johnson, P. Lake, E.J. McGuire, T.A. Mehlorn, T.D. Pointon, T.J. Rank, W.A. Stygar, Y. Maron, and E. Stambulchik, *Laser Part. Beams* **14**, 543 (1996).
 - [7] T. Fujimoto and S.A. Kazantsev, *Plasma Phys. Controlled Fusion* **39**, 1267 (1997).
 - [8] J.R. Oppenheimer, *Z. Phys.* **43**, 27 (1927).
 - [9] I.C. Percival and M.J. Seaton, *Philos. Trans. R. Soc. London* **251**, 113 (1958).
 - [10] U. Fano and J.H. Macek, *Rev. Mod. Phys.* **45**, 553 (1973).
 - [11] M.K. Inal and J. Dubau, *J. Phys. B* **20**, 4221 (1987).
 - [12] J.C. Kieffer, J.P. Matte, M. Chaker, Y. Beaudoin, C.Y. Chien, S. Coe, G. Mourou, J. Dubau, and M.K. Inal, *Phys. Rev. E* **48**, 4648 (1993).
 - [13] A.S. Shlyaptseva, I.E. Golovkin, and U.I. Safronova, *J. Quant. Spectrosc. Radiat. Transf.* **56**, 157 (1996).
 - [14] P. Beiersdorfer, D.A. Vogel, K.J. Reed, V. Decaux, J.H. Scofield, K. Widmann, G. Hölzer, E. Förster, O. Wehrhan, D.W. Savin, and L. Schweikhard, *Phys. Rev. A* **53**, 3974 (1996).
 - [15] A.S. Shlyaptseva, R.C. Mancinin, P. Neill, and P. Beiersdorfer, *Rev. Sci. Instrum.* **68**, 1095 (1997).
 - [16] T. Fujimoto and M. Nakai, in *Proceedings of the International Seminar on Atomic Processes in Plasmas NIFS-PROC-44, 2000* (unpublished), p. 77.
 - [17] M.E. Cuneo, P.R. Menge, D.L. Hanson, W.E. Fowler, M.A. Bern, R. Ziska, A.B. Filuk, J.E. Bailey, M.P. Desjarlais, T.R.

- Lockner, Mehlhorn, T.D. Pointon, S.A. Slutz, M.A. Stark, and R.A. Vesey, *IEEE Trans. Plasma Sci.* **25**, 229 (1997).
- [18] A.B. Filuk, J.E. Bailey, A.L. Carlson, D.J. Johnson, P. Lake, T.A. Mehlhorn, L.P. Mix, T.J. Renk, W.A. Stygar, and Y. Maron, *Phys. Rev. Lett.* **77**, 3557 (1996).
- [19] T.J. Renk, R.G. Buchheit, N.R. Sorensen, D. Cowell Senft, M.O. Thompson, and K.S. Grabowski, *Phys. Plasmas* **5**, 2144 (1998).
- [20] C. Litwin and Y. Maron, *Phys. Fluids B* **1**, 670 (1989).
- [21] J.E. Bailey, A.L. Carlson, R.L. Morrison, and Y. Maron, *Rev. Sci. Instrum.* **61**, 3075 (1990).
- [22] J.E. Bailey, R. Adams, A.L. Carlson, C.H. Ching, A.B. Filuk, and P. Lake, *Rev. Sci. Instrum.* **68**, 1009 (1997).
- [23] R.L. Coldwell and G.J. Bamford, *The Theory and Operation of Spectral Analysis Using ROBFIT* (AIP, New York, 1991).
- [24] J.C. Weisheit and B.W. Shore, *Astrophys. J.* **194**, 519 (1974).
- [25] C. Lanczos, *Z. Phys.* **62**, 518 (1930).
- [26] C.E. Moore, *Atomic Energy Levels*, Natl. Bur. Stand. Ref. Data Ser., Nat. Bur. Stand. (U.S.) (U.S. GPO, Washington, D.C., 1971), Vol. I.
- [27] I. Bray, *Phys. Rev. A* **49**, 1066 (1994).
- [28] R. Shingal, *J. Phys. B* **21**, 125 (1988).
- [29] R. Odom, J. Caddick, and J. Weiner, *Phys. Rev. A* **14**, 965 (1976).
- [30] D.R. Schultz (private communication).
- [31] R.K. Janev (private communication).
- [32] J. Schweinzer (private communication).